Tonks-Girardeau gas in different potential traps by exact diagonalization

Abel Vicenç Yuste Roca
*Facultat de Física, Universitat de Barcelona, Diagonal 645, 08028 Barcelona, Spain.**

Advisors: M.A. Garcia-March, A. Polls
(Dated: July 23, 2014)

We computed the second-quantized many-mode Hamiltonian for spinless ultracold bosons trapped in different one-dimensional potentials and diagonalized it for a small number of atoms. We observed the transition from the non-interacting gas to the Tonks-Girardeau gas, i.e. the fermionization process, as we increase the strength of the interactions between the atoms. We computed the energy spectrum, the one-body density matrix, the two-body correlations, the momentum distribution, the natural orbitals and the occupations for different interaction strengths. We compared the fermionization in different potentials with special attention to the largest occupation of the natural orbits, the build up of quantum many-body correlations between different parts of the system, and the energy of the ground and excited states.

I. INTRODUCTION

The first experimental realizations of a Bose-Einstein condensate (BEC) [1, 2] paved the way for a huge number of research lines, both theoretical and experimental, on the area of ultracold quantum gases. Ultracold atoms provide a system highly isolated from the environment. Moreover, this is an extremely versatile system because the geometry of the trapping potential and the interparticle forces can be externally controlled. Thus, they opened the possibility to reproduce condensed matter phenomena in artificial systems. For example, the quantum phase transition from a superfluid to a Mott insulator was experimentally observed with ultracold bosons trapped in a periodic external potential [3].

In these systems, the transverse degrees of freedom can be frozen and the system can be regarded effectively as one dimensional (1D) [4, 5]. Moreover, the interparticle interactions can be well controlled by means of Feshbach or confinement induced resonances [6]. For weakly interacting regimes, the system is well described by the Gross-Pitaevskii theory which is a mean field approach [9]. In this regime, the atoms are said to be Bose-Einstein condensed, as they mainly occupy the lowest natural orbital. The opposite regime, with infinite repulsive contact interactions, is the so called Tonks-Girardeau (TG) regime. In here, the system maps to non-interacting fermions, as the infinite repulsive interactions for bosons play a similar role than the Pauli exclusion principle for fermions [10]. However, this resemblance between the highly interacting bosons and the non-interacting fermions exists only for some quantities such as the total energy and the density profile, while other quantities such as the momentum distribution differ completely [10, 11]. The experimental realization of a TG gas in a single trap or in a periodic optical lattice was recently reported [7, 8].

In this work, we will study this kind of system for different trapping potentials paying special attention to the transition from the non-interacting to the TG gas, transition also known as fermionization process. We analize quantities such as the one- and two-body correlations, the energy spectrum, the momentum distribution or the occupation of the orbitals. To treat these kind of systems, different numerical approaches have been performed, for instance, the Multi-Configuration Time-Dependent Hartree method [12–14], which is computationally costly and permits one only to study the ground state. Here, instead, we are going to use an exact diagonalization study like in Ref. [15]. The disadvantage of this method is that we have to truncate the mode expansion and use a few number of atoms in order to keep a numerically manageable dimension of the Fock space.

The work is organized as follows. In Sec. II, a brief description of the Hamiltonian of the system is provided. We also discuss the mapping between the many body system of bosons and the corresponding non-interacting fermion system in the case of an infinite repulsive contact force. All the definitions, in first and second quantization, of the different operators and observables considered in the work are also presented. In Sec III, the relevant computational details are explicitly discussed. In Sec IV, the results are provided for the different trapping potentials considered. Finally, in Sec V, the conclusions of this work are summarized.

II. THEORETICAL FRAMEWORK

The following Hamiltonian in first quantization

$$\hat{\mathcal{H}} = \hat{\mathcal{H}}_0 + V_{2body}, \tag{1}$$

where $\hat{\mathcal{H}}_0$,

$$\hat{\mathcal{H}}_0 = \sum_{i=1}^{N} [-\frac{\hbar^2}{2m}\frac{\partial^2}{\partial z_i^2} + V(z_i)], \tag{2}$$

describes a system of N spinless 1D bosons trapped in an external trap. The two-body contact interaction is

* abelcech@gmail.com

modeled by a delta potential of the form

$$V_{2body} = g\sum_{i,j}^{N}\delta(z_i - z_j), \tag{3}$$

where the coupling constant g is the strength of the delta force. For $g \to \infty$, we get a system of hard core bosons because the potential V_{2body} can be seen as a constraint in the wave function $\psi(z_1, z_2, ..., z_N)$ of the form

$$\psi = 0 \quad \text{if} \quad |z_i - z_j| = 0, \quad 1 \leq i < j \leq N. \tag{4}$$

The constraint in Eq. (4) is always satisfied by the wave function of non-interacting fermions because of antisymmetry requirements. In this way, the Fermi-Bose mapping theorem [10] tells that, in this limit, the ground state for bosons, ψ^B_{GS}, can be written as:

$$\psi^B_{GS} = |\psi^F_{GS}|, \tag{5}$$

where ψ^F_{GS} is the wave function for non-interacting fermions and solution of $\hat{\mathcal{H}}_0$. Note that ψ^F_{GS} is given by the Slater determinant

$$\psi^F_{GS}(z_1, z_2, ..., z_N) = \frac{1}{\sqrt{N!}}\begin{vmatrix} \phi_1(z_1) & ... & \phi_1(z_N) \\ \vdots & \ddots & \vdots \\ \phi_N(z_1) & ... & \phi_N(z_N) \end{vmatrix}, \tag{6}$$

where the $\phi_i(z)$ are the eigenfunctions of the single-particle Hamiltonian,

$$H_{sp} = -\frac{1}{2}\frac{\partial^2}{\partial z^2} + V(z). \tag{7}$$

and in the following they are called modes. A bosonic system fulfilling Eq. (5) is the so called TG gas.

In second quantization, the Hamiltonian in Eq. (1) with the interaction in Eq. (3) can be written as [16]

$$\hat{\mathcal{H}} = \int dz\hat{\psi}^\dagger(z)H_{sp}\hat{\psi}(z) + \frac{g}{2}\int dz\hat{\psi}^\dagger(z)\hat{\psi}^\dagger(z)\hat{\psi}(z)\hat{\psi}(z). \tag{8}$$

We use harmonic oscillator length and energy scales, and therefore, the energy will be in $\hbar\omega$ units and the distances in harmonic oscillator length, $l_z = \sqrt{\frac{\hbar}{m\omega}}$. Here m and ω are the mass of the atom and the trapping frequency respectively. We can expand the field operators $\hat{\psi}(z)$ as a linear combination of M modes

$$\hat{\psi}(z) = \sum_{n=1}^{M}\hat{a}_n\phi_n(z), \tag{9}$$

where the creation and annihilation operators $\hat{a}^\dagger_k$ and $\hat{a}_k$ satisfy the bosonic commutation relations $[\hat{a}^\dagger_k,\hat{a}_i]=\delta_{ik}$ and $[\hat{a}^\dagger_k,\hat{a}^\dagger_i]= [\hat{a}_k,\hat{a}_i]=0$. Therefore, the many-particle Hamiltonian built with M single-particle modes reads [15]

$$\hat{\mathcal{H}} = \sum_i E_i\hat{a}^\dagger_i\hat{a}^\dagger_i + \frac{g}{2}\sum_{i,j,k,l} I_{i,j,k,l}\hat{a}^\dagger_i\hat{a}^\dagger_j\hat{a}_k\hat{a}_l, \tag{10}$$

where $I_{i,j,k,l} = \int_{-\infty}^{+\infty} dz\phi_i(z)\phi_j(z)\phi_k(z)\phi_l(z)$ and E_i are the single particle energies associated to H_{sp}. $I_{i,j,k,l}$ has units of $[1/l_z]$, and so g has units of $[\hbar\omega_z l_z]$ and tells us how strong the contact interaction is. Once we compute this Hamiltonian we diagonalize it,

$$\hat{\mathcal{H}}|\psi_n(z)\rangle = E_n|\psi_n(z)\rangle, \tag{11}$$

and obtain the eigenvectors $\hat{\psi}(z)_n$ with energies E_n. To begin with, let us consider the ground state eigenvector $\hat{\psi}_1(z) \equiv \hat{\psi}_{GS}(z)$ with energy E_{GS}.

The non-diagonal one-body density matrix is defined as

$$\rho^{(1)}(z, z') \equiv \langle\hat{\psi}^\dagger(z')\hat{\psi}(z)\rangle_{GS} = \sum_{i,j}\langle\hat{a}^\dagger_i\hat{a}_j\rangle_{GS}\phi_i(z)\phi_j(z'), \tag{12}$$

which diagonal $\rho(z) \equiv \rho^{(1)}(z, z)$ gives us the particle density profile. In order to get the momentum distribution, we must perform a Fourier transform of $\rho^{(1)}(z, z')$

$$n(k) = (2\pi)^{-1}\int_{-\infty}^{+\infty} dz\int_{-\infty}^{+\infty} dz'\rho^{(1)}(z, z')e^{-ik(z-z')}. \tag{13}$$

On the other hand, $\rho^{(1)}(z, z')$ can also be diagonalized as

$$\rho^{(1)}(z, z') = \sum_i N_i f_i(z')^* f_i(z), \tag{14}$$

where f_i are the natural orbitals and N_i their occupations, which fulfill: $\sum_i N_i = N$. The average occupation of the single-particle modes is

$$\langle n_i\rangle = \langle a^\dagger_i a_i\rangle, \tag{15}$$

which is also normalized to N. We will also study the existence of two-body correlations. The definition of the diagonal two-body density matrix is

$$\begin{aligned}\rho^{(2)}(z_1, z_2) &\equiv \langle\hat{\psi}^\dagger(z_1)\hat{\psi}^\dagger(z_2)\hat{\psi}(z_2)\hat{\psi}(z_1)\rangle_{GS} = \\ &= \langle\hat{a}^\dagger_i\hat{a}^\dagger_j\hat{a}_k\hat{a}_l\rangle_{GS}\phi_i(z_1)\phi_j(z_2)\phi_k(z_1)\phi_l(z_2),\end{aligned} \tag{16}$$

which we will also refer as two-body distribution function. We have also computed the analytic form of $\rho^{(1)}(z, z')$ and $\rho^{(2)}(z_1, z_2)$ for the TG limit. This is done by using the analytic expression of $\psi^B_{GS}(z_1, z_2, ..., z_n)$ in terms of the absolute value of the Slater determinant given in Eq.(6) and using the first quantization expressions [11]:

$$\begin{aligned}\rho^{(1)}(z, z') = N\int &\psi^B_{GS}(z, z_2, ..., z_N) \\ &\times\psi^B_{GS}(z', z_2, ..., z_N)dz_2...dz_N,\end{aligned} \tag{17}$$

$$\rho^{(2)}(z_1, z_2) = N(N-1)\int |\psi^B_{GS}(z_1, z_2, ..., z_N)|^2 dz_3...dz_N. \tag{18}$$

We will also make an analysis of the energy decomposition for the harmonic oscillator case. The energy consists of three terms

$$E_t = E_{kin} + E_{pot} + E_{int}. \tag{19}$$

The first term, E_{kin}, is the kinetic energy and is related to the momentum distribution as

$$E_{kin} = \frac{\langle n(k)^2 \rangle_{GS}}{2}. \tag{20}$$

The second term, E_{pot}, is the trapping potential energy which can be obtained from the density profile with

$$E_{pot} = \frac{\langle z^2 \rangle_{GS}}{2}. \tag{21}$$

Finally, the last term, E_{int}, can be obtained by means of the two-body distribution function

$$E_{int} = \frac{g}{2} \int dz \rho^{(2)}(z,z). \tag{22}$$

However, we have only computed both E_{kin} and E_{pot} and obtained E_{int} as $E_{int} = E_t - E_{kin} - E_{pot}$.

Finally, we check if the virial theorem is fulfilled for the harmonic oscillator trap and $N = 2$. To derive the virial theorem, we scale an eigenstate of the Hamiltonian as

$$\psi'(z_1, z_2) = \lambda \psi(\lambda z_1, \lambda z_2). \tag{23}$$

Then, we compute the expectation value of the Hamiltonian for the new wave function ψ'

$$E(\lambda) = \langle \psi' | \frac{1}{2}(-\frac{\partial^2}{\partial z_1^2} - \frac{\partial^2}{\partial z_2^2} + z_1^2 + z_2^2) + g\delta(z_1 - z_2) | \psi' \rangle. \tag{24}$$

Making use of the variational principle, we impose that $E(\lambda)$ has a minimum at $\lambda = 1$. In this way, we can obtain the virial expression which gives a relation between the three energy terms

$$2E_{kin} - 2E_{osc} + E_{int} = 0. \tag{25}$$

This expression should be fulfilled for all g. In particular, if we consider the case $g = 0$, i.e. $E_{int} = 0$, we obtain the virial theorem for the harmonic oscillator, $E_{kin} = E_{osc}$. Otherwise, if we consider $g \to \infty$ fermionization takes place and, according to Eq. (4), two atoms cannot be in the same position giving again $E_{int} = 0$ and $E_{kin} = E_{osc}$. For intermediate values of g, E_{int} is not zero and Eq. (25) must be fulfilled.

III. NUMERICAL METHODS

As a first step, we compute the Fock basis for N number of atoms and a given number of single-particle modes, M. That means defining all possible vectors that arrange the N particles in M modes which we write as: $|n_1, n_2, ..., n_M\rangle$. For instance, for $N = M = 2$, the Fock basis is

$$|20\rangle, |11\rangle, |02\rangle. \tag{26}$$

The dimension of the Fock space, D, is the combination with repetitions between N and M,

$$D = \begin{pmatrix} M+N-1 \\ N \end{pmatrix}. \tag{27}$$

For a given N, we have to choose a proper M in order not to have a too large D that would require extremely long computational time and memory. At the same time we have to study the convergence of the results depending on the truncation of the modes expansion. For instance, we have chosen $N = 2$, $M = 25$ and $N = 3$, $M = 15$ giving 325 and 560 Fock vectors respectively. Some calculations with larger Fock basis have been performed so as to check the numerical convergence of the method.

Next, we build the Hamiltonian given in Eq. (10). The first term is easily computed because is diagonal. The two-body interaction generates non-diagonal matrix elements whose computation requires a lot of two-body matrix elements. In order to reduce computational time, a first program computes all the terms needed for a given Fock basis. This program computes all the possible values of i, j, k, l that contribute in the two-body interactions, $\langle \hat{a}_i^\dagger \hat{a}_j^\dagger \hat{a}_k \hat{a}_l \rangle$, and their respective coefficients. This number of two-body matrix elements increases strongly with N and M, for instance, for $N = 3$ and $M = 15$ the number of terms is $\sim$ 300.000. We just have to calculate these coefficients once and store them. Then, one can easily compute both the interacting part of $\hat{\mathcal{H}}$ and $\rho^{(2)}(z_1, z_2)$.

Another program solves the Schrödinger equation for H_{sp} using a finite difference method. The outputs are the single-particle wave functions ϕ_i and the single-particle energy spectrum E_i. This program also computes the integrals $I_{i,j,k,l}$ which are required in Eq. (10).

Then, diagonalizing $\hat{\mathcal{H}}$, we get the N-particle energy spectrum and the eigenvectors, $\psi_n(z)$. With this information, we can compute $\rho^{(1)}(z, z')$ and $\rho^{(2)}(z_1, z_2)$. We can obtain the rest of outputs from $\rho^{(1)}(z, z')$. For instance, the natural orbitals f_i are obtained by diagonalizing $\rho^{(1)}(z, z')$ or the momentum distribution, $n(k)$ by means of Eq. (13).

IV. RESULTS

We restrict the spatial domain to $z \in [-10, 10]$ and discretize this domain with a step of $\delta = 0.01$. Due to the computational limitations, most of the simulations are for $N = 2$. Nevertheless, calculations with $N = 3$ are

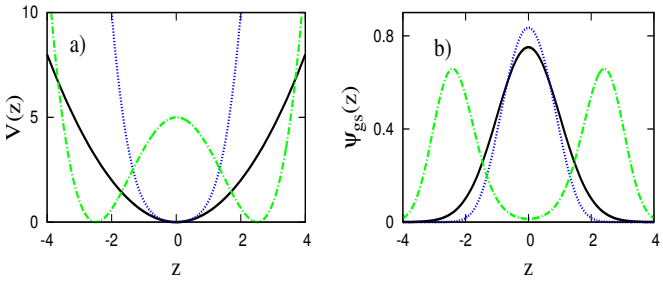

FIG. 1. The potentials V(z) used in the calculations are plotted in (a) and the respective single-particle ground state wave function ψ_{gs} solving the Schrödinger equation without interactions in (b). The potentials have the form of Eq. (28), with $\alpha = 1$, $\beta = 0$ for the harmonic (solid black line), $\alpha = 1$, $\beta = 0.5$ for the anharmonic (dotted blue line) and the Duffing form [see Eq. (29)] with $V_0 = \Delta = 5$ for the double well, (dash-dotted green line).

also reported. The traps considered have the form

$$V(z) = \frac{1}{2}\alpha z^2 + \beta z^4. \tag{28}$$

In Fig. 1(a), the different trapping potentials are plotted. For the harmonic trap, we use $\alpha = 1$, $\beta = 0$. Raising β we obtain a more squeezed trap (i.e., $\alpha = 1$, $\beta = 0.5$). To have a double well, we can change the sign of α. The characteristic parameters of a double well are the height of the barrier between the two wells: V_0 and the distance between the minimums, Δ. In order to have a better control over these two parameters, we have used, instead of Eq. (28), the so-called Duffing potential

$$V(z) = V_0(\frac{-8}{\Delta^2}z^2 + \frac{16}{\Delta^4}z^4 + 1), \tag{29}$$

which allows us to choose V_0 and Δ and sets the value of the potential at the minimums at 0. An example of a Duffing potential is also plotted in Fig. 1(a) with $V_0 = \Delta = 5$.
The single-particle ground state ψ_{gs} for these three potentials are plotted in Fig. 1(b) where we can observe that the initial Gaussian profile characteristic of the harmonic oscillator potential gets thinner when the potential is squeezed. In the double well, due to the potential barrier the wave function has a minimum at the origin and two symmetric maximums take place at the center of each well.

A. Harmonic Trap

We have made calculations for different values of g. For small values we obtain a behavior close to a non-interacting Bose gas while for $g \sim 20$ we approach the TG regime. The several computed observables allow to do an analysis of this transition and the TG's properties.

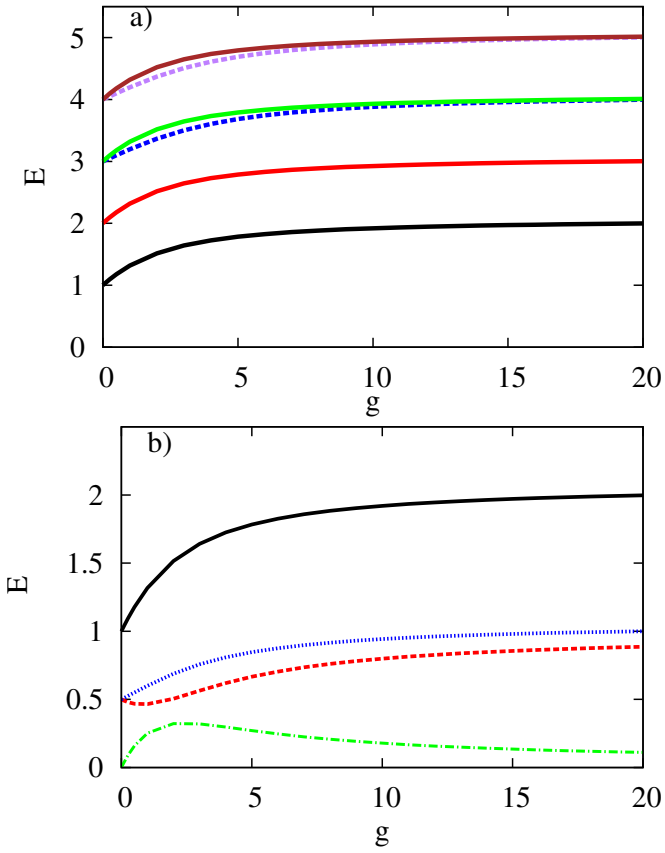

FIG. 2. In panel (a), the first six values of the energy spectrum for $N = 2$. For clarity, we use a dashed-line where there are two degenerate states for $g = 0$. We can observe fermionization, i.e., reaching the TG energy, at $g \sim 20$. In panel (b), the energy of the ground state is decomposed in E_{kin} (dashed red line), E_{osc} (dotted blue line) and E_{int} (dash-dotted green line).

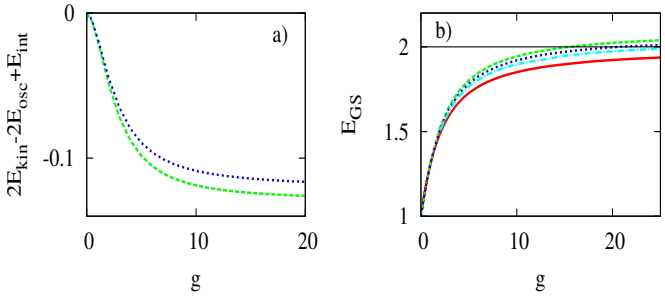

FIG. 3. The virial theorem [left side of Eq. (25)] is plotted in panel (a) for different g and 25 modes (dashed green line) and 15 modes (dotted blue line). We see that, as we increase g, it deviates from 0 and hence, the virial is not exactly fulfilled. This deviation is smaller as we increase the number of modes. In panel (b), the ground state energy E_{GS} for 15 and 25 modes [same label as in panel (a)], 50 modes (dash-dotted cyan) and the analytical one (solid red line) obtained in [17].

1. *Energy analysis*

In Fig. 2 (a), for $N = 2$, the energy spectrum shows that for small g, we have the spectrum of a non-interacting Bose gas, i.e., with the sequence $E_i = 1, 2, 3, 3, 4, 4, ...$ As we increase g, a transition towards TG regime takes place. For $g \sim 20$, the energy tends to that of a non-interacting gas of trapped fermions, i.e. $E = 2, 3, 4, 4, 5, 5...$ At $g = 0$, some trivial degeneracies appear in the spectrum, which are slightly broken as g increases. Some of the excited states can be identified with excitations of the center of mass motion. For these states, the energy distance respect to the state without this excitation does not depend on g, i.e., on the interaction term. In the other cases the excitations are associated to the relative motion which depends on the interaction term. In the limit $g \to \infty$, when the interaction energy is 0, one again recovers the degeneracies but with larger values of the energy [17].

In Fig. 2(b), we show in detail the three components of the energy, E_{kin}, E_{pot} and E_{int} as we detailed in Eq. (19). Note that E_{int} shows a maximum at $g \sim 2$ and after that decreases as g increases. In the limit $g \to \infty$, E_{int} becomes 0 because two atoms cannot be in the same position, and therefore, the expectation value of the contact interaction is 0. Furthermore, in this limit, $E_{kin} = E_{pot} = 1$ fulfilling the virial theorem (25). The fact that $E_{int} \approx 0$ is another criteria for considering that fermionization has taken place.

Let us study the error due to the truncation in the mode expansion. In Fig. 3(a), the left side of Eq. (25) is plotted as a function of g for 15 and 25 modes. The value should be 0 for all g, instead, it decreases from 0 at $g = 0$ to ~ -0.1 for larger g. This error is larger as we increase g because more modes are needed to have a proper computation, since there are more non-negligible terms in the Hamiltonian involving the upper levels. To check that, in Fig. 3(b) we show the ground state energy, E_{GS} as a function of g for different number of modes compared with the analytic value computed in Ref. [17]. We can see that the energy that we obtain is always larger than the analytical one and that the calculated energy is more accurate as we increase the number of modes. This fact can be understood taking into account the variational property of the diagonalization method. We have as a trial wave function a linear combination of a finite number of Fock vectors. Solving the Schrödinger equation of the truncated Hamiltonian, we obtain the coefficients that give us the best energy which will be always an upper bound of the exact one. If we increase the number of modes, the trial wave function is closer to the exact one and so the energy gets closer to the analytical one too. However, this convergence is rather slow as it can be seen in Fig. 3(b).

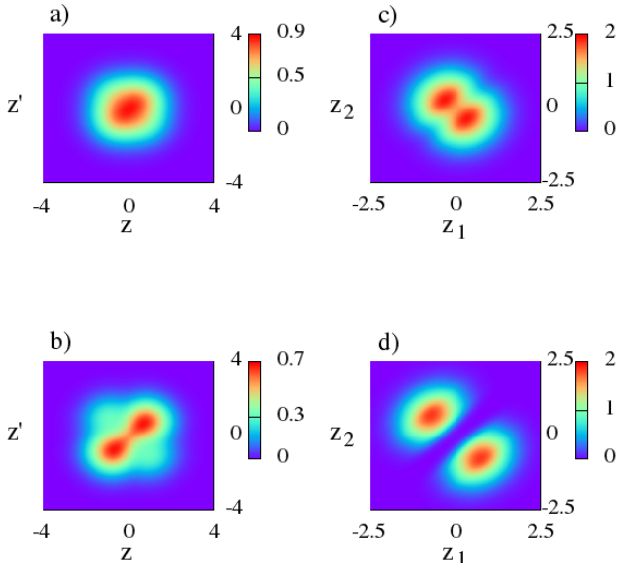

FIG. 4. $\rho^{(1)}(z, z')$ is plotted for the cases $g = 2$ in (a) and $g = 20$ in (b). For small g, in (a), $\rho^{(1)}(z, z')$ still resembles a Gaussian. For large g, in (b), $\rho^{(1)}(z, z')$ takes the form of a TG gas. The panels (c) and (d) show the two-body distribution function $\rho^{(2)}(z_1, z_2)$ for $g = 1$ and $g = 20$ respectively. Notice that $\rho^{(2)}(z, z) \approx 0$ for $g = 20$.

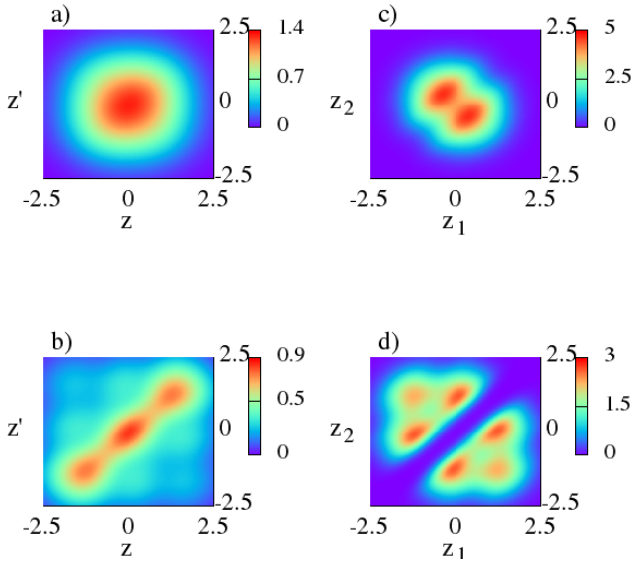

FIG. 5. Same plot as in Fig. 4 for $N = 3$.

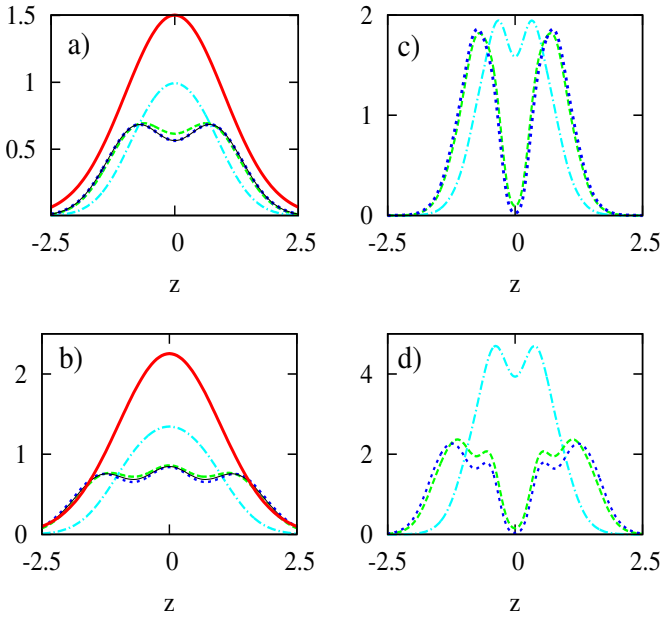

FIG. 6. The density profile, $\rho(z)$, is plotted for $N = 2$ (a) and for $N = 3$ (b) for $g = 0$ (thin solid red line), $g = 1$ (dash-dotted cyan line), $g = 10$ (dashed green line), $g = 20$ (dotted blue) and the analytic TG limit (thin solid black line). For small values of g, we get a Gaussian profile. As we increase g, the profile flattens until that it has the same form as the TG limit for $g \sim 20$. The two-body distribution function, $\rho^2(z, -z)$, is plotted for $N = 2$ (c) and for $N = 3$ (d) for $g = 1$, 10 and 20 with the same labels as in panels (a) and (b). We observe that for large g it decays to 0 at $z_1 = z_2 = 0$ because two atoms cannot be in the same place.

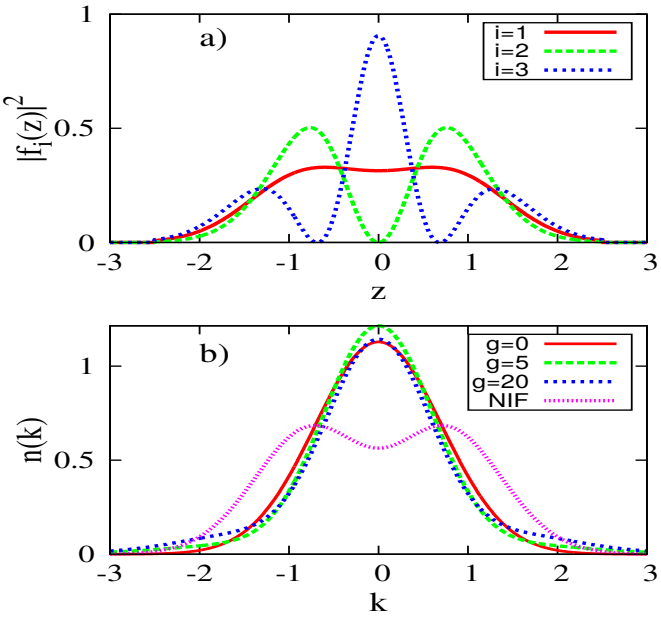

FIG. 7. In (a), the modulus square of the first three natural orbitals, $|f_i(z)|^2$, are plotted for $g = 20$. Panel (b) shows the momentum distribution for different values of g and the analytical one for non-interacting fermions (NIF). Notice that this momentum distributions are normalized to the number of atoms.

2. *One- and two-body correlations*

In Fig. 4(a) and (b), $\rho^1(z, z')$ is plotted for $g = 2$ and $g = 20$ respectively and $N = 2$. The same is done for $N = 3$ in Fig. 5(a) and (b). The initial Gaussian form in (a) changes towards the characteristic density profile of a TG gas with strong off-diagonal correlations [11]. This transition is clearly appreciated in Fig. 6 (a) and (b), where the diagonal $\rho^{(1)}(z, z) \equiv \rho(z)$ is plotted for $N = 2$ and $N = 3$ respectively for several values of g. The initial $\rho(z)$ of non-interacting bosons (NIB), $\rho(z)_{NIB} = N\phi_{gs}^2(z)$, $\rho(z)$ flattens to obtain the non-interacting fermion profile (NIF), $\rho(z)_{NIF} = \sum_{i=1}^{N} \phi_i^2(z)$. This NIF profile is already reached at $g \sim 20$.

$\rho^2(z_1, z_2)$ is showed in Fig. 4(c) and (d) for $N = 2$ and in Fig. 5(c) and (d) for $N = 3$, for $g = 1$ and $g = 20$ respectively. We observe that increasing g, $\rho^2(z, z)$ becomes zero. This is because two atoms cannot be in the same place as a direct consequence of the infinity interaction potential. For more clarity, we have plotted $\rho^{(2)}(z, -z)$ in Fig. 6(c) and (d). We can observe that the behavior of the two-body correlations evolves faster than the one-body ones, and that from $g = 10$ the profile is already near 0 at $z_1 = z_2$ having a similar form as for $g = 20$.

3. *Momentum distribution and natural orbitals*

From $\rho^{(1)}(z, z')$, we can obtain the natural orbitals $f_i(z)$ and the momentum distribution $n(k)$ with Eq. (14) and (13) respectively. Fig. 7 shows, for $N = 2$, the first three $f_i(z)$ for $g = 20$ in (a) and the momentum distribution, $n(k)$, in (b) for different values of g. We can observe that $n(k)$ does not change appreciably as we increase g although the corresponding $\rho(z)$ is completely different [see Fig. 6(a)]. On the other hand, the NIF momentum distribution is completely different from that of the TG. We can also observe that the high momentum tail of the TG momentum distribution decays more slowly than for low g, indeed, $n(k) \propto 1/k^4$ in accordance with the predictions in Ref. [18, 19].

Finally, the single-particle average occupation of the mode i, $\langle n_i \rangle$, and the natural orbital occupation, N_i, are shown in Fig. 8 (a) and (b) respectively for $N = 2$. For small values of g, the occupation is restricted to the lowest single-particle state, and therefore we have a large condensate fraction, defined as the largest occupation of the natural orbitals. As we increase the interaction, more single-particle states are occupied. Nevertheless, the occupation distribution is not that of NIF, i.e. $\langle n_i \rangle = 1$ in the N first levels, and 0 in the upper ones. Instead, we observe a large value of the occupation of the lowest single-particle state and non zero values of $\langle n_i \rangle$ for $i > N$. On the other hand, the ground state natural occupation fulfill the condition $N_{GS} \approx N^{-0.41}$ obtained in Ref. [11].

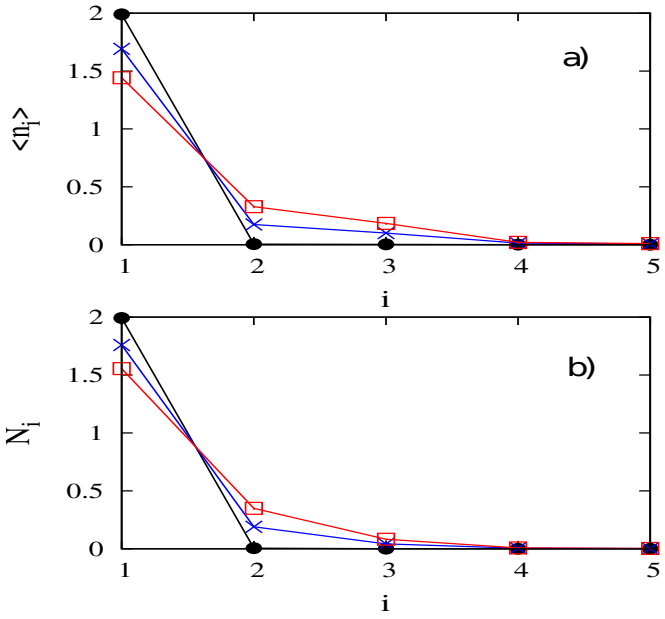

FIG. 8. The average single-particle occupations, $\langle n_i \rangle = \langle a_i^\dagger a_i \rangle$ (a), and the natural orbital occupations N_i (b), are plotted for $g = 0.5$ (squares), $g = 5$ (crosses) and $g = 20$ (circles) for $N = 2$. They have a similar behavior filling more excited orbitals as we increase g.

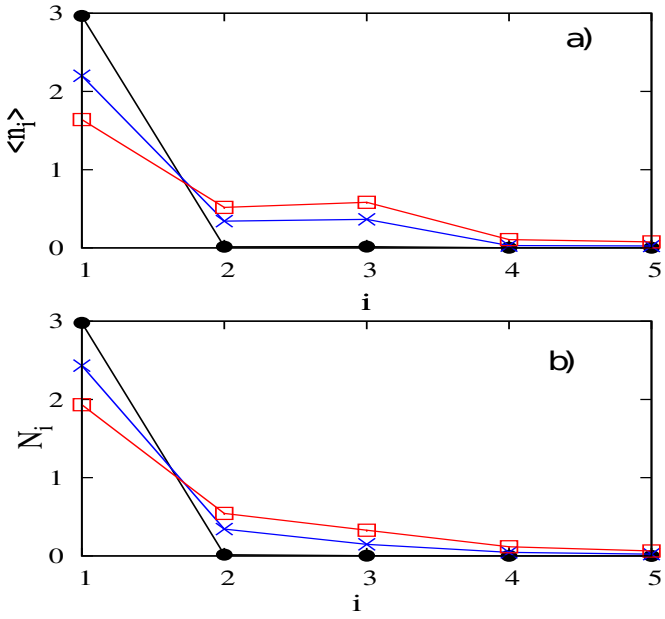

FIG. 9. Same plot and labels as in Fig. 8 for $N = 3$. We observe that for the average single-particle occupations, $\langle n_i \rangle = \langle a_i^\dagger a_i \rangle$, the second excited state is more occupied than the first one.

Another thing that can be easily observed is that this redistribution of the NIB occupation as we increase g is stronger for $\langle n_i \rangle$ than for N_i. For instance, for $i = 3$ and $g = 20$ $\langle n_3 \rangle \sim 0.3$ and $N_3 \sim 0.1$.
In Fig. 9, we plot the single-particle average occupation and the natural orbitals occupations for $N = 3$. In here, we observe that the second excited single-particle state is more occupied than the first one for $g = 20$. In fact, this is a general characteristic of the TG gas that the even states are in proportion more occupied than the odd ones [15].

B. Anharmonic Trap

If we raise the parameter β in Eq. (28) while α is kept constant, the central profile of the trap does not change but the potential grows more quickly as we increase z. In Fig. 10(a), the trap for $\beta = 0.5$ is compared with the harmonic oscillator one. The respective eigenvalues are shown as horizontal lines. We can see that this squeezing of the potential raises and separates the single-particle eigenvalues with respect to those from the harmonic oscillator. In the TG gas regime, the ground state is obtained from the absolute value of the Slater determinant which, for $N = 2$, is

$$\psi_{GS}^B = |\phi_1(x_1)\phi_2(x_2) - \phi_1(x_2)\phi_2(x_1)|, \qquad (30)$$

where ϕ_1 and ϕ_2 are the numerically calculated eigenfunctions of the anharmonic potential with eigenvalues E_1 and E_2, which differ from those of the harmonic trap. Therefore, the energy in the TG limit is $E_{TG} = E_1 + E_2$, which corresponds to NIFs trapped in this potential. In Fig. 10(b), E_{TG} as a function of β is plotted. We can see that E_{TG} increases as we raise β as a consequence of having larger single-particle eigenvalues E_1 and E_2. In this case, the fermionization process needs larger values of g, as shown in Fig. 11, where the ground state energy for different β are plotted as a function of g. As β is increased, the energy tends more slowly to the corresponding E_{TG}. For instance, for $\beta = 0$ (the case studied in the preceding section), the E_{TG} energy is practically reached at $g = 30$. Instead, for $\beta = 10$ the energy is around 5% smaller at the same value of g.

$\rho^{(1)}(z, z')$ and $\rho^{(2)}(z_1, z_2)$ for $\beta = 10$ and $N = 2$ are plotted in Fig. 12(a) and (c), respectively. To compute them, we used the TG analytical limit, [see Eq. (30)] and the first quantization expressions in Eq. (18). We can see that the shape is similar to the harmonic case, being more squeezed in the anharmonic potential. To observe better this behavior, we plot in Fig. 12(b) and (d) the densities $\rho(z) = \rho^{(1)}(z, z)$ and $\rho^{(2)}(z_1, -z_1)$ for $\beta = 10$, and compare with the harmonic oscillator results. The profiles have similar shapes but the harmonic oscillator one is wider. However, the TG gas for $\beta = 10$ has approximately the same natural occupations distribution, N_i, as in the harmonic oscillator. This effect can be seen in Fig. 13(a) where the natural orbitals occupations are plotted for the harmonic trap and the anharmonic one for $\beta = 10$. Nevertheless, the momentum distribution $n(k)$ plotted in Fig. 13(b) differs completely between the different traps and, as we observed in Fig. 7(b), differs

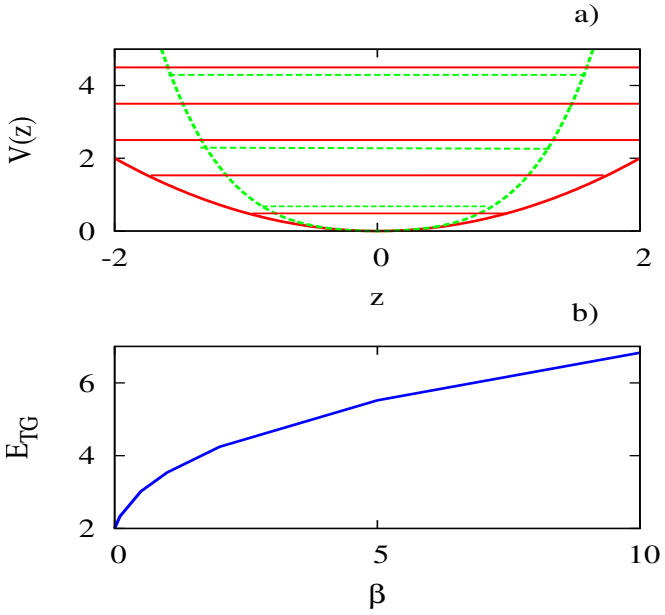

FIG. 10. In panel (a) the harmonic potential (solid red line) and the anharmonic one for $\beta = 0.5$ (dashed green line). Horizontal lines represent the respective single-particle energies. In panel (b), we plot the energy of the Tonks-Girardeau gas for $N = 2$, $E_{TG} = E_1 + E_2$, as a function of β.

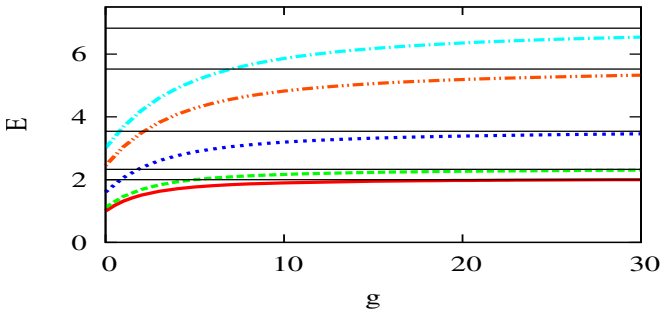

FIG. 11. Ground state energy as a function of the interaction energy g for different β and $N = 2$. The values of β are 0 (solid thick red line), 0.1 (dashed green line), 1 (dotted blue line) , 5 (dash-dotted-dotted line) and 10 (dash-dotted cyan line). As a guide to the eye, we also plot an horizontal black line at the respective value of E_{TG}.

also from the respective NIF momentum distribution.

C. Double well

Finally, we consider a Duffing double well potential [see Eq. (29)] with the parameters $V_0 = \Delta = 5$ [see Fig. 1 (a)]. These parameters produce a quite high barrier and, therefore, the single-particle eigenvalues of this double well are quasi-degenerate by pairs, i.e. $E_1 \simeq E_2 < E_3 \simeq E_4 < ...$

The first seven eigenvalues of the energy spectrum of the system with $N = 2$ are shown in Fig. 14 as a function

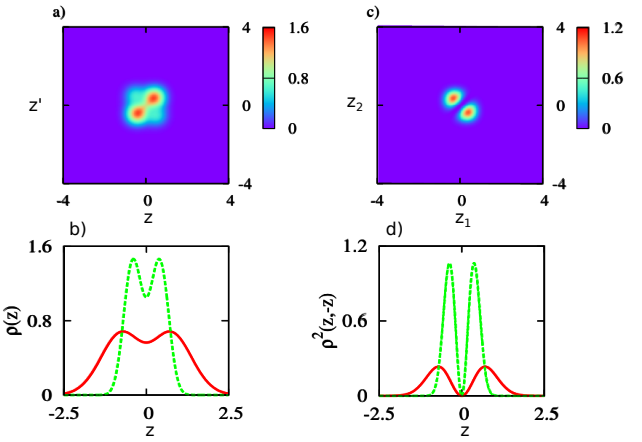

FIG. 12. One- and two-body densities, $\rho^1(z, z')$ (a) and $\rho^2(z_1, z_2)$ (c), for $\beta = 10$ in the TG limit. A similar profile as the harmonic oscillator but more squeezed as we can see in $\rho(z)$ (b) and in $\rho^2(z, -z)$ (d), where the values for $\beta = 10$ (dash green line) are compared with those of the harmonic oscillator (solid red line).

of g. For $g = 0$, we have three states which are almost degenerate, they correspond to the Fock states: $|2, 0, ...\rangle$, $|1, 1, 0, ...\rangle$ and $|0, 2, 0, ...\rangle$. Their energy is basically twice the lowest single-particle eigenvalue, $E(g = 0) \approx 2E_1$. When g increases, the quasi-degeneracy is lost and the ground state (with no degeneracy) has an energy which is practically independent of g. That is because it is not sensitive to the interaction energy. In the Fock basis, and for $g \neq 0$, this ground state is: $C(|20\rangle - |02\rangle)$ where C is a normalization constant. The energy of the other states grows as we raise g keeping their degeneracy and reaching an asymptotic value in which they do not feel the interaction anymore. In this limit, they merge with other two states which energy does not depend on g.

The density profile of the ground state, $\rho_{GS}(z)$, for $g = 1, 10$ and 20 is plotted in Fig. 15. One can appreciate that the profile does not depend on the value of g and that the two atoms are equally distributed in the two wells. However, two clarify whether the interaction affects the energy of this state, we report in Fig. 16 the two-body distribution function, $\rho^{(2)}(z_1, z_2)$, for $g = 20$. In fact, $\rho^{(2)}(z, z) = 0$ and, therefore, the expectation value of the interaction energy is zero in this state [see Eq. (22)].

In this case, we can say that there is no fermionization in the ground-sate. The existence of the two quasi-degenerate single-particle states of different parity, allows a ground state whose two-body distribution function has zeros when two atoms occupy the same position. Of course, that will depend on the height of the barrier, V_0. When we sufficiently decrease it, fermionization will take place because there will be contact interaction between the atoms. In addition, it is almost certain that fermionization will take place in some of the excited states probably giving a TG at each size of the chain.

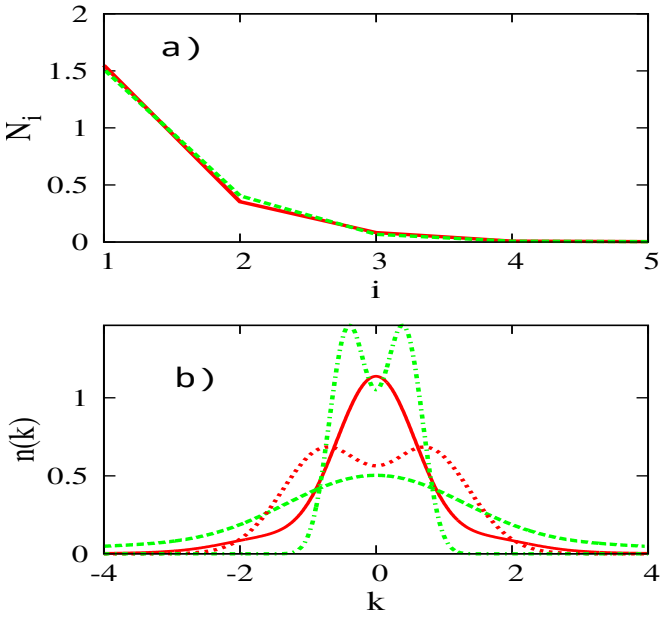

FIG. 13. TG exact natural occupations, N_i, for $\beta = 10$ (dashed green line) and for the harmonic oscillator (solid red line) are plotted in (a). In panel (b) we report the momentum distribution n(k) for the TG limit for $\beta = 10$ (dashed green line) and for harmonic oscillator (solid red line). There are also plotted the NIF n(k) for $\beta = 10$ (dash-dotted green line) and harmonic oscillator (dotted red line).

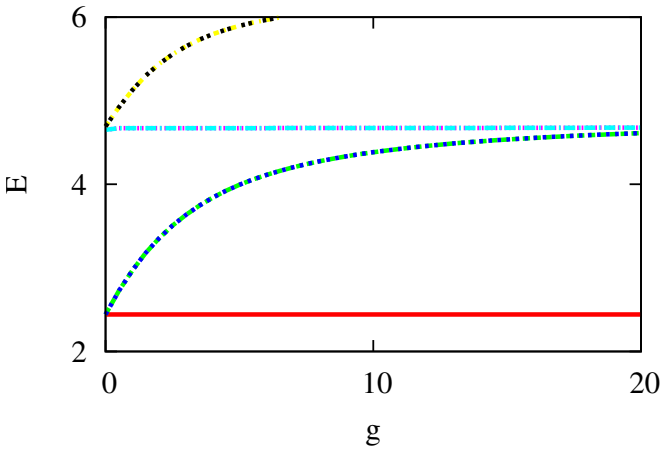

FIG. 14. Energy spectrum for the Duffing double well with $V_0 = \Delta = 5$, as a function of g. The seven first eigenvalues are shown. The ground state (solid red line) is constant, and then the levels are degenerated by pairs.

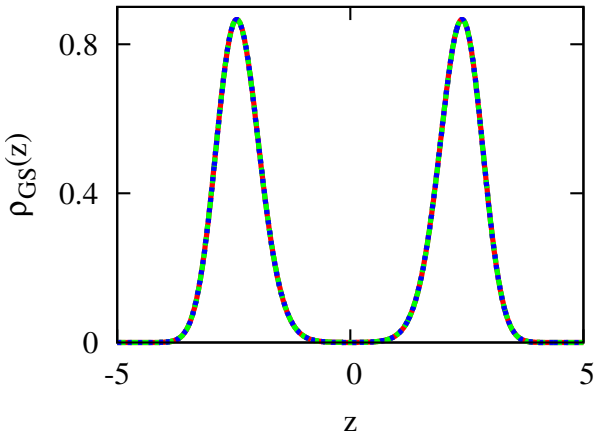

FIG. 15. Density profile for the ground state, $\rho_{GS}(z)$ for $g = 1$ (solid red line), $g = 10$ (dash green line) and $g = 20$ (dotted blue line). For $\rho_{gs}(z)$. The three profiles overlap

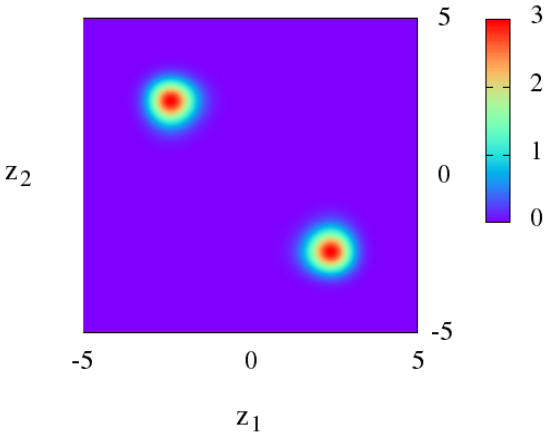

FIG. 16. Two-body distribution function for the ground state, $\rho^{(2)}_{GS}(z_1, z_2)$, and $g = 20$. We can observe that its diagonal, $\rho^{(2)}_{GS}(z, z)$, is zero.

V. CONCLUSIONS

We performed an extensive numerical study about the transition, commonly known as fermionization, from the non-interacting gas of bosons to the Tonk-Girardeau gas trapped by harmonic, anharmonic and double well potentials. We used a computational method based in the diagonalization of a many-mode expansion of the second-quantized Hamiltonian. We studied the error introduced by the truncation in the number of modes used in the expansion of the second-quantized fields. For the harmonic potential, we observe the Tonks-Girardeau behavior at a coupling constant $g \approx 20\hbar\omega l_z$, where ω is the trapping frequency and l_z the harmonic oscillator length. In this limit, the one- and two-body densities coincide with the analytic limit obtained by Girardeau *et. al.*, with the Fermi-Bose mapping theorem [11]. Moreover, the parti-

cle density is the same as the one corresponding to non-interacting fermions. However, other quantities like the momentum distribution and the natural orbital occupations differ completely, due to the different symmetrization condition for fermions and bosons.

We also studied the transition from the non-interacting gas of bosons to the Tonks-Girardeau gas in the anharmonic potential obtained by considering a parabolic contribution and a quartic one in the total trapping potential. We demonstrated that the Tonks-Girardeau limit equally exist for this potential and used an analytical expression for the first-quantized wave function in this limit. We conclude that the existence of the Tonks-Girardeau gas does not depend on an equal spacing between the energetic levels. We showed that a similar transition as that observed for the harmonic trap takes place between the non-interacting and Tonks-Girardeau limits as g is increased, but it requires larger values of the interaction strength because the energetic space between the single-particle eigenvalues is larger than in the harmonic trap. The one- and two-body densities have a similar shape as those calculated for the harmonic potential but they are more spatially concentrated in the center of the trap. The natural orbital occupation distribution in the Tonks-Girardeau regime is approximately the same as in the harmonic case, while their momentum distributions differ, due to the different form of the single-particle modes.

Finally, we considered a double well potential constructed by adding an inverted parabola and a quartic potential, resembling a Duffing potential. We showed that the ground state energy, density profile and two-body distribution function do not depend on the g considered. In this way, the ground state does not show a fermionization process. However, this phenomena will depend on the height of the barrier. It would be very interesting to study the existence of fermionization on the excited states but this goes beyond the scope of the present work.

VI. ACKNOWLEDGMENTS

The author is specially grateful to M.A.Garcia-March and A.Polls for the continuous support and guidance during the realization of this work and to Bruno Julià Díaz for useful discussions.

[1] C. C. Bradley *et al.*, Phys. Rev. Lett. **75**, 9 (1995).
[2] K. B. Davis *et al.*, Phys. Rev. Lett. **75**, 22 (1995).
[3] M. Greiner *et al.*, Nature 415, 39 (2002).
[4] D. Blume, Rep. Prog. Phys. **75**, 046401 (2012).
[5] I. Bloch and W. Zwerger, Rev. Mod. Phys. **80**, 885 (2008).
[6] M. Olshanii, Phys. Rev. Lett. **81**, 938 (1998).
[7] B. Paredes *et al.*, New J. Phys. **12**, 093041 (2010).
[8] T. Kinoshita, T.Wenger an D. S. Weiss, Science 305, 1125 (2004).
[9] L. Pitaevskii and S. Stringari, *Bose-Einstein Condensation* (Oxford University Press,Oxford,2003).
[10] M. Girardeau, J. Math. Phys. **1**, 516 (1960).
[11] M. Girardeau, E. M. Wright, and J. M. Triscari, Phys. Rev. A **63**,033601 (2001).
[12] L. S. Cederbaum and A. I. Strelsov, Phys. Lett. A 318, 564 (2003).
[13] O. E. Alon and L. S. Cederbaum, Phys. Rev. Lett. 95, 140402 (2005).
[14] S. Zöllner, H. D. Meyer, and P. Schmelcher, Phys. Rev. A 74, 063611 (2006).
[15] F.Deuretzbacher, K.Bongs, K.Sengstock, and D.Pfannkuche. Phys.Rev.A 75,013614 (2007).
[16] Alexander L. Fetter, John Dirk Walecka, *Quantum Theory of Many-particle Systems*, McGraw-Hill, (1971).
[17] T. Busch *et al.*, Foundations of Physics, Vol.28,549 (1997).
[18] G. J. Lapeyre, Jr., M. D. Girardeau, and E. M. Wright, Phys. Rev. A, **66**, 023606 (2002).
[19] A. Minguzzi, P. Vignolo,M. P. Tosi, Physics Letters A, 294, 222 (2002).